Universidad Carlos III de Madrid

e-Archivo

Institutional Repository

A robust observer based on energy-to-peak filtering in combination with neural networks for parameter varying systems and its application to vehicle roll angle estimation[☆]

B.L. Boada[*], M.J.L. Boada, V. Diaz

Mechanical Engineering Department, Research Institute of Vehicle Safety (ISVA), Universidad Carlos III de Madrid, 30 Leganés, Madrid 28911, Spain

A B S T R A C T

This paper presents a robust observer based on energy-to-peak filtering in combination with a neural network for vehicle roll angle estimation. Energy-to-peak filtering estimates the minimised error for any bounded energy disturbance. The neural network acts as a 'pseudo-sensor' to estimate a vehicle 'pseudo-roll angle', which is used as the input for the energy-to-peak-based observer. The advantages of the proposed observer are as follows. 1) It does not require GPS information to be utilised in various environments. 2) It uses information obtained from sensors that are installed in current vehicles, such as accelerometers and rate sensors. 3) It reduces computation time by avoiding the calculation of observer gain at each time sample and utilising a simplified vehicle model. 4) It considers the uncertainties in parameters of the vehicle model. 5) It reduces the effect of disturbances. Both simulation and experimental results demonstrate the effectiveness of the proposed observer.

1. Introduction

Currently, rollover accidents account for approximately 33% of all motor vehicle deaths [1]. To reduce the occurrence of this type of accident is one of the main objectives in the design of vehicle control systems [2]. Vehicle control systems that aim to improve vehicle rollover behaviour are called roll stability control (RSC) systems.

The majority of RSC systems require knowledge of vehicle roll angle to calculate lateral load transfer and properly coordinate control systems. Vehicle roll angle can be directly measured using a GPS dual-antenna. The disadvantage of this technique is that it is very costly. For this reason, vehicle roll angle should be estimated.

However, the estimation of vehicle roll angle must be performed in real time using the sensors installed on-board in current vehicles to achieve acceptable RSC controller performance [3].

In [4] and [5], GPS information was fused with information obtained from sensors installed in vehicles, such as inertial navigation system (INS) sensors, wheel speed sensors, and steering angle sensors.

The problem with using GPS is the difficulty in achieving accurate readings because of the limited visibility of satellites in both urban and forested driving environments. In [6], vehicle roll angle was estimated using information from suspension deflection sensors and a lateral accelerometer. However, this technique does not provide accurate results

[7] and is very costly because the required sensors are typically not installed in vehicles.

In [8], a dynamic vehicle roll angle observer that fuses information obtained from a lateral accelerometer and gyroscope was designed. However, the drawback of this algorithm is that the estimated vehicle roll angle transient response contains a crucial error.

A common method used to fuse information from different sensors is the Kalman filter. In [7,9–11], a Kalman filter was utilised to estimate vehicle roll angle. The drawbacks of using a Kalman filter are as follows: 1) the model and measurement noises must be known, 2) the vehicle model must be precise, and 3) the gain matrix must be calculated at each time sample. If the first condition is not met, the performance of the Kalman filter may be degraded [12]. Additionally, the last condition leads to increased computation time.

To handle system uncertainties and varying parameters, a robust observer and controller must be designed. In [13–15], robust controllers were proposed to improve the lateral behaviour of a vehicle. Robust observers have also been proposed to estimate vehicle sideslip angle, [16,17] and vehicle longitudinal velocity [18]. However, there is a lack of research on the design of a robust observer related to vehicle roll angle.

The majority of previous methods use physical models for the estimation of vehicle states. However, when a model has nonlinear

characteristics and parameters are difficult to determine, as in the case of vehicles, one potential solution is the use of artificial intelligence. In [19] and [20], vehicle sideslip angle was estimated using a neural network (NN) and adaptive neural fuzzy inference system (ANFIS). In [7], an NN was used for vehicle roll angle estimation. The problem in these methods is that sensor noise strongly affects variable estimation. In [7] and [21], integration of an ANFIS and NN with a Kalman filter was performed for estimating vehicle sideslip angle and vehicle roll angle, respectively. In these works, improved results for the ANFIS and NN were obtained when a Kalman filter was combined with previous methodologies.

Considering the aforementioned disadvantages of the Kalman filter, we focus on the development of a robust observer based on energy-to-peak filtering in combination with an NN for vehicle roll angle estimation. Energy-to-peak filtering estimates the minimised error for any bounded energy disturbance.

The design of our observer is based on the following criteria:

- To facilitate system use in all types of environments, we must not use GPS information.
- Utilise information obtained from sensors that are installed in current vehicles, such as accelerometers and rate sensors.
- Reduce computation time by avoiding the calculation of observer gain at each time sample and utilising a simplified vehicle model.
- The proposed algorithm must be usable in different road conditions.
- We must consider the uncertainties in parameters of the vehicle model.
- We must attenuate the effects of external disturbances.

The remainder of this paper is organised as follows. Section 2 describes the vehicle model used by the proposed observer. Section 3 introduces the observer architecture that is formed by an 'NN module' and 'energy-to-peak filtering module'. In Section 4, simulation and experimental results are presented to verify the effectiveness of the proposed observer. Finally, our conclusions are summarised in Section 5.

2. Vehicle model

In this study, a one degree-of-freedom vehicle model, as shown in Fig. 1, is used to describe vehicle roll motion. A detailed description of
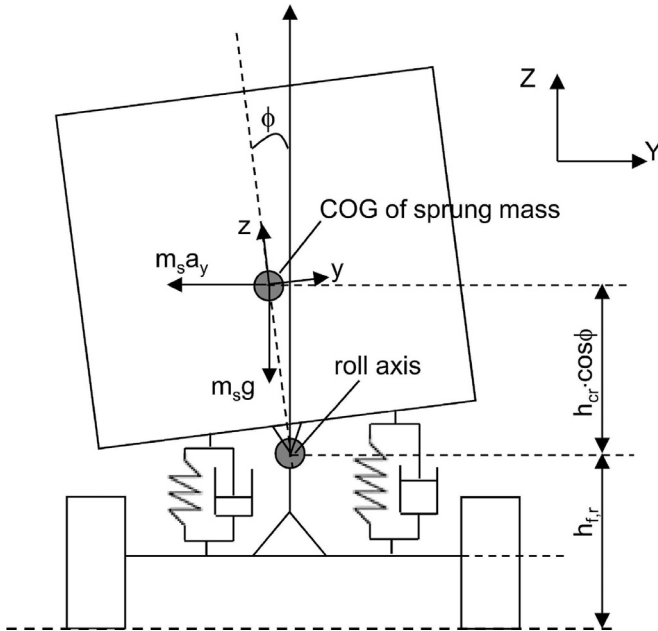

Fig. 1. Vehicle roll model.

this model can be found in [7].

A linear parameter varying (LPV) model of the vehicle roll dynamic can be represented as:

$$\dot{\mathbf{x}}_0 = (\mathbf{A}_0 + \Delta\mathbf{A}_0)\mathbf{x}_0 + (\mathbf{B}_0 + \Delta\mathbf{B}_0)\mathbf{a}_{ym} + \mathbf{H}\mathbf{w} \tag{1}$$

$$\mathbf{y}_{meas} = \mathbf{C}_0\mathbf{x}_0 + \mathbf{q}, \tag{2}$$

where $\mathbf{x}_0$ is the state vector, $[\phi, \dot{\phi}]^T$, ϕ is the vehicle roll angle, $\dot{\phi}$ is the vehicle roll rate, $\mathbf{y}_{meas}$ is the measurement vector, a_{ym} is the lateral acceleration measured by a sensor at the centre of gravity (COG) of the vehicle, $\mathbf{w}$ is the unknown and bounded external disturbance, $\mathbf{q}$ is the measurement noise, and $\Delta\mathbf{A}_0$ and $\Delta\mathbf{B}_0$ represent the system uncertainties for the matrices $\mathbf{A}_0$ and $\mathbf{B}_0$, respectively:

$$\mathbf{A}_0 + \Delta\mathbf{A}_0 = \begin{bmatrix} 0 & 1 \\ \dfrac{-(K_R + \Delta K_R)}{(I_{xx} + \Delta I_{xx})} & \dfrac{-(C_R + \Delta C_R)}{(I_{xx} + \Delta I_{xx})} \end{bmatrix}$$

$$\mathbf{B}_0 + \Delta\mathbf{B}_0 = \begin{bmatrix} 0 \\ \dfrac{(m_s + \Delta m_s)(h_{cr} + \Delta h_{cr})}{(I_{xx} + \Delta I_{xx})} \end{bmatrix} \tag{3}$$

I_{xx} is the sprung mass moment of inertia with respect to the roll axis, m_s is the sprung mass, h_{cr} is the sprung mass height about the roll axis, C_R represents the total torsional damping, K_R is the stiffness coefficient, g is the acceleration due to gravity, and ΔK_R, ΔC_R, Δh_{cr}, and Δm_s are the maximum uncertainties of K_R, C_R, h_{cr}, and m_s, respectively. $\mathbf{C}_0$ is the output matrix:

$$\mathbf{C}_0 = \begin{bmatrix} 1 & 0 \\ 0 & 1 \end{bmatrix} \tag{4}$$

and, finally,

$$\mathbf{H} = \mathbf{I}_{2x2} \tag{5}$$

To simply analyse, the following considerations have been taken into account:

$$\frac{m + \Delta m}{n + \Delta n} = \frac{m}{n + \Delta n} + \frac{\Delta m}{n + \Delta n} \approx \frac{m}{n} + \frac{\Delta m}{n} \tag{6}$$

$$(m + \Delta m)(n + \Delta n) = mn + m\Delta n + \Delta mn + \Delta m\Delta n$$
$$\approx mn + m\Delta n + \Delta mn \tag{7}$$

Then, the uncertainty matrices can be rewritten as:

$$\Delta\mathbf{A}_0 = \mathbf{E}_A \cdot \mathbf{M}_A \cdot \mathbf{F}_A \tag{8}$$

$$\Delta\mathbf{B}_0 = \mathbf{E}_B \cdot M_B \cdot \mathbf{F}_B \tag{9}$$

where

$$\mathbf{E}_A = \begin{bmatrix} 0 & 0 \\ \frac{-\Delta K_R}{I_{xx}} & \frac{-\Delta C_R}{I_{xx}} \end{bmatrix} \tag{10}$$

$$\mathbf{F}_A = \mathbf{I}_{2x2} \tag{11}$$

$$\mathbf{E}_B = \begin{bmatrix} 0 \\ \frac{\Delta m_s h_{cr} + m_s \Delta h_{cr}}{I_{xx}} \end{bmatrix} \tag{12}$$

$$\mathbf{M}_A = \begin{bmatrix} N(t) & 0 \\ 0 & N(t) \end{bmatrix} \tag{13}$$

$$\mathbf{M}_B = N(t) \tag{14}$$

$$|N(t)| \leq 1 \tag{15}$$

$$\mathbf{F}_B = \mathbf{I}_{1x1} \tag{16}$$

3. Vehicle roll angle observer design

In this section, our vehicle roll angle observer is described. Fig. 2
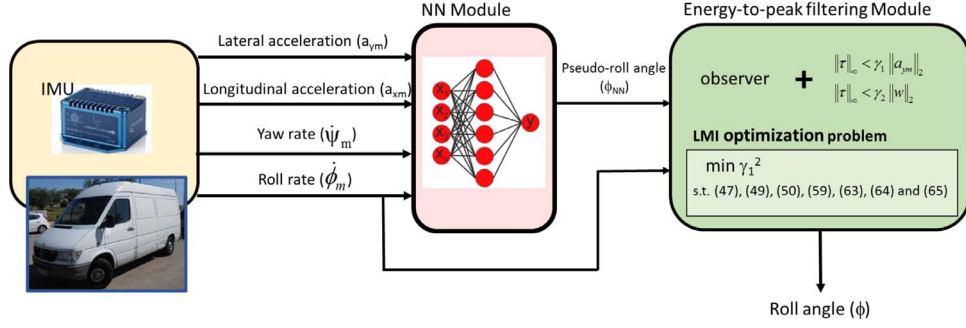
2

Fig. 2. Architecture of the vehicle roll angle observer.

illustrates the proposed observer architecture. This architecture is formed by two modules. The former module, called the 'NN module', uses a multilayer perceptron (MLP) NN for data fusion from inertial measurement unit (IMU) signals to estimate a vehicle 'pseudo-roll angle'.

The latter module, called the 'energy-to-peak filtering module', receives the 'pseudo roll angle' estimated by the NN module and roll rate obtained directly from the IMU as inputs. This module is used to reduce noise in the inputs and obtain a better estimation of vehicle roll angle. In contrast to the Kalman filter, the energy-to-peak filter does not require knowledge regarding sensor noise. Another advantage of the proposed algorithm is that because the output of the NN module only depends on inputs and is not time-dependent, analysis of convergence in the proposed algorithm (NN + energy-to-peak observer) is reduced to analysing only the convergence of the energy-to-peak observer, unlike the state estimators for NNs proposed in [22] and [23].

The following subsections provide detailed descriptions of these modules.

3.1. NN module

The NN module utilises a static artificial NN to calculate a 'pseudo-roll angle' using the signals from an IMU sensor. The NN module then acts as a 'pseudo-sensor' that provides a measurement of the roll angle. The IMU sensor, which is installed at the COG of the vehicle, measures longitudinal, lateral, and vertical accelerations, as well as yaw, roll, and pitch rates. These signals are referred to the coordinate reference system of the IMU. The MLP NN architecture designed for estimation of the 'pseudo-roll angle' is presented in Fig. 3. The NN is formed by a single hidden layer with 15 neurons, four inputs corresponding to the longitudinal acceleration a_{xm}, lateral acceleration a_{ym}, yaw rate $\dot{\psi}_m$, and roll rate $\dot{\phi}_m$ and one output corresponding to the vehicle 'pseudo-roll angle', ϕ_{NN}.

The training of the MLP NN is performed using a backpropagation algorithm. The training patterns were obtained by using a vehicle simulation model from TruckSim [24], which has been validated using real test data. The NN is trained for different types of manoeuvres, which allows it to characterise vehicle behaviours, such as lane changes

(LCs), double lane changes (DLCs), and J-turns, for different speeds (ranging from 30 km/h to 140 km/h) and road friction coefficients (0.3: ice, 0.5: wet, and 1: dry).

The NN parameters, consisting of synaptic weights (w_{ji} and w_{1j}) and biases (b_j and c), have been tuned based on an error signal e and according to the generalised delta rule. The error signal is defined as:

$$e = \phi_d - \phi_{NN} \tag{17}$$

where ϕ_d is the desired vehicle roll angle obtained from the TruckSim vehicle model and ϕ_{NN} is the estimated vehicle roll angle from the NN. The training process stops when the synaptic weights and bias levels in the network stabilise and the average squared error over the entire training set converges to some minimum value. A detailed description of the training process for NNs and the results obtained are provided in [7].

One of the main advantages of the NN module is that the 'pseudo-roll angle' is obtained directly from sensor signals without performing any integration. Therefore, there is no accumulated error in the estimation. Another advantage is that the signals used as inputs for the NN module are provided by sensors that are installed in current vehicles equipped with ABS and ESP systems.

3.2. Energy-to-peak filtering module

The energy-to-peak filtering module estimates the vehicle roll angle using the 'pseudo-roll angle' estimated by the previous module and yaw rate provided by the IMU sensor as inputs. During energy-to-peak filtering, estimation error is minimised for any bounded energy disturbance.

The system defined in Section 2 depends on the sensor lateral acceleration a_{ym} and external disturbance $\mathbf{w}$. In order to reduce the effects of both inputs on roll angle estimation, the energy-to-peak performance is defined as [13,16,25]:

$$\begin{aligned} \|\tau\|_\infty &< \gamma_1 \|a_{ym}\|_2 \\ \|\tau\|_\infty &< \gamma_2 \|\mathbf{w}\|_2 \end{aligned}, \tag{18}$$

where τ is the output observer (see Eqs. (28) and (44)), γ_1 is the performance index, and γ_2 is a weighting factor that determines the
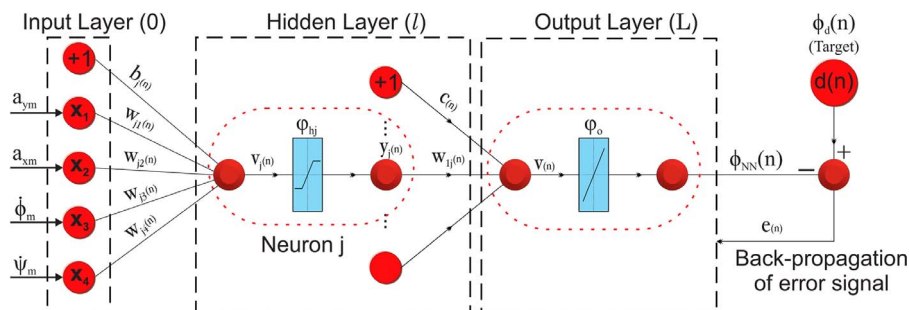

Fig. 3. Observer architecture.

relative importance of the effects of the two external inputs, a_{ym} and $\mathbf{w}$, on the estimated error in the output ϕ.

The energy-to-peak performance will be verified by two different observers. The same variables are defined for both observers in order to use the equations provided in Section 3.2.3.

3.2.1. Observer 1

The first observer is utilised to prove that the energy-to-peak performance is given by Zhang et al. [16]:

$$\dot{\hat{\mathbf{x}}}_0 = \mathbf{A}_0\hat{\mathbf{x}}_0 + \mathbf{B}_0 a_{ym} + \mathbf{L}_0(\mathbf{y}_{meas} - \mathbf{C}_0\hat{\mathbf{x}}_0), \tag{19}$$

where $\mathbf{y}_{meas}$ is the sensor or 'pseudo-sensor' data. Therefore, $\mathbf{y}_{meas} = \mathbf{C}_0\mathbf{x}_0 + \mathbf{q}$ (see Eq. (2)) and $\mathbf{L}_0$ is the observer gain to be calculated.

The estimation error of a state is defined as:

$$\mathbf{e} = \mathbf{x}_0 - \hat{\mathbf{x}}_0 \tag{20}$$

Therefore, the estimation error dynamic can be calculated as:

$$\dot{\mathbf{e}} = \dot{\mathbf{x}}_0 - \dot{\hat{\mathbf{x}}}_0 \tag{21}$$

By substituting Eqs. (1) and (19) into Eq. (21) and performing the calculations, we obtain:

$$\dot{\mathbf{e}} = (\mathbf{A}_0 - \mathbf{L}_0\mathbf{C}_0)\mathbf{e} + \Delta\mathbf{A}_0\mathbf{x}_0 + \Delta\mathbf{B}_0 a_{ym} + \mathbf{Hw} + \mathbf{L}_0\mathbf{q} \tag{22}$$

Because matrix $\mathbf{H}$ is the identity matrix, the above equation can be rewritten as:

$$\dot{\mathbf{e}} = (\mathbf{A}_0 - \mathbf{L}_0\mathbf{C}_0)\mathbf{e} + \Delta\mathbf{A}_0\mathbf{x}_0 + \Delta\mathbf{B}_0 a_{ym} + \mathbf{H}(\mathbf{w} + \mathbf{L}_0\mathbf{q}) \tag{23}$$

The term $(\mathbf{w} + \mathbf{L}_0\mathbf{q})$ is bounded if the system is asymptotically stable because; in this case, $\mathbf{L}_0$ exists and is bounded. Therefore, the external disturbance vector is given by:

$$\mathbf{w}' = \mathbf{w} + \mathbf{L}_0\mathbf{q} \tag{24}$$

A new state vector $\xi = [\mathbf{e}, \mathbf{x}_0]^T$ is defined as:

$$\dot{\xi} = \mathbf{A}_p\xi + \mathbf{B}_p a_{ym} + \mathbf{H}_p\mathbf{w}', \tag{25}$$

where $\mathbf{w}'$ is an unknown bounded external disturbance vector and:

$$\mathbf{A_p} = \begin{bmatrix} (\mathbf{A}_0 - \mathbf{L}_0\mathbf{C}_0) & \Delta\mathbf{A}_0 \\ \mathbf{0}_{2x2} & \mathbf{A}_0 + \Delta\mathbf{A}_0 \end{bmatrix} = \begin{bmatrix} (\overline{\mathbf{A}} - \mathbf{L}\overline{\mathbf{C}}) & \Delta\overline{\mathbf{A}} \\ \mathbf{0}_{2x6} & \mathbf{A}_0 + \Delta\mathbf{A}_0 \end{bmatrix}$$

$$\mathbf{B}_p = \begin{bmatrix} \Delta\mathbf{B}_0 \\ \mathbf{B}_0 + \Delta\mathbf{B}_0 \end{bmatrix} = \begin{bmatrix} \Delta\overline{\mathbf{B}} \\ \mathbf{B}_0 + \Delta\mathbf{B}_0 \end{bmatrix}$$

$$\mathbf{H}_p = \begin{bmatrix} \mathbf{H} \\ \mathbf{H} \end{bmatrix} = \begin{bmatrix} \overline{\mathbf{H}} \\ \mathbf{H} \end{bmatrix} \tag{26}$$

By substituting the uncertainty terms into the function for the time-varying matrix $\mathbf{M}$, we obtain:

$$\mathbf{A}_p = \begin{bmatrix} (\overline{\mathbf{A}} - \mathbf{L}\overline{\mathbf{C}}) & \mathbf{E}_A\mathbf{M}_A\mathbf{F}_A \\ \mathbf{0}_{2x6} & \mathbf{A}_0 + (\mathbf{E}_A\mathbf{M}_A\mathbf{F}_A) \end{bmatrix} = \begin{bmatrix} (\overline{\mathbf{A}} - \mathbf{L}\overline{\mathbf{C}}) & \overline{\mathbf{E}}_A\mathbf{M}_A\mathbf{F}_A \\ \mathbf{0}_{2x6} & \mathbf{A}_0 + (\mathbf{E}_A\mathbf{M}_A\mathbf{F}_A) \end{bmatrix}$$

$$\mathbf{B}_p = \begin{bmatrix} \mathbf{E}_B\mathbf{M}_B\mathbf{F}_B \\ \mathbf{B}_0 + (\mathbf{E}_B\mathbf{M}_B\mathbf{F}_B) \end{bmatrix} = \begin{bmatrix} \overline{\mathbf{E}}_B\mathbf{M}_B\mathbf{F}_B \\ \mathbf{B}_0 + (\mathbf{E}_B\mathbf{M}_B\mathbf{F}_B) \end{bmatrix} \tag{27}$$

Because the roll angle is the signal to be estimated, the performance of proposed observer is evaluated based on its error estimation:

$$\tau = \mathbf{G}\xi, \tag{28}$$

with $\mathbf{G} = [1 \quad 0 \quad 0 \quad 0]$.

3.2.2. Observer 2

The second proposed observer is based on the Luenberger observer [26]. In this case, we consider sensor measurements that are contaminated by sensor biases. Therefore, the output is filtered as:

$$\dot{\mathbf{z}} = \mathbf{Fz} + \mathbf{y}_{meas} = \mathbf{Fz} + \mathbf{C}_0\mathbf{x}_0 + \mathbf{q}, \tag{29}$$

where $\mathbf{F}$ is the filter gain.

Based on the systems described by Eqs. (1) and (29), a new state vector $[\mathbf{x}_0, \mathbf{z}]^T$ is defined as:

$$\begin{bmatrix} \dot{\mathbf{x}}_0 \\ \dot{\mathbf{z}} \end{bmatrix} = \begin{bmatrix} \mathbf{A}_0 + \Delta\mathbf{A}_0 & \mathbf{0}_{2x2} \\ \mathbf{C}_0 & \mathbf{F} \end{bmatrix}\begin{bmatrix} \mathbf{x}_0 \\ \mathbf{z} \end{bmatrix} + \begin{bmatrix} \mathbf{B}_0 + \Delta\mathbf{B}_0 \\ \mathbf{0}_{2x1} \end{bmatrix}a_{ym} + $$
$$+ \begin{bmatrix} \mathbf{I}_{2x2} \\ \mathbf{0}_{2x2} \end{bmatrix}\mathbf{w} + \begin{bmatrix} \mathbf{0}_{2x2} \\ \mathbf{I}_{2x2} \end{bmatrix}\mathbf{q} \tag{30}$$

The new output vector is defined as the filtered output signal:

$$\mathbf{Y} = \begin{bmatrix} \mathbf{0}_{2x2} & \mathbf{I}_{2x2} \end{bmatrix}\begin{bmatrix} \mathbf{x}_0 \\ \mathbf{z} \end{bmatrix} \tag{31}$$

Then,

$$\dot{\mathbf{X}} = (\mathbf{A} + \Delta\mathbf{A})\mathbf{X} + (\mathbf{B} + \Delta\mathbf{B})a_{ym} + \mathbf{H}_X\mathbf{w} + \Phi\mathbf{q},$$
$$\mathbf{Y} = \mathbf{CX} \tag{32}$$

where

$$\mathbf{A} = \begin{bmatrix} \mathbf{A}_0 & \mathbf{0}_{2x2} \\ \mathbf{C}_0 & \mathbf{F} \end{bmatrix}$$

$$\Delta\mathbf{A} = \begin{bmatrix} \Delta\mathbf{A}_0 & \mathbf{0}_{2x2} \\ \mathbf{0}_{2x2} & \mathbf{0}_{2x2} \end{bmatrix}$$

$$\mathbf{B} = \begin{bmatrix} \mathbf{B}_0 \\ \mathbf{0}_{2x1} \end{bmatrix}$$

$$\Delta\mathbf{B} = \begin{bmatrix} \Delta\mathbf{B}_0 \\ \mathbf{0}_{2x1} \end{bmatrix}$$

$$\mathbf{H}_X = \begin{bmatrix} \mathbf{I}_{2x2} \\ \mathbf{0}_{2x2} \end{bmatrix}$$

$$\Phi = \begin{bmatrix} \mathbf{0}_{2x2} \\ \mathbf{I}_{2x2} \end{bmatrix}$$

$$\mathbf{C} = \begin{bmatrix} \mathbf{0}_{2x2} & \mathbf{I}_{2x2} \end{bmatrix} \tag{33}$$

Considering the newly defined state vector, the proposed observer has the following form:

$$\dot{\hat{\mathbf{X}}} = \mathbf{A}\hat{\mathbf{X}} + \mathbf{B}a_{ym} + \Phi\hat{\mathbf{p}} + \mathbf{L}_0(\mathbf{Y} - \mathbf{C}\hat{\mathbf{X}})$$
$$\dot{\hat{\mathbf{p}}} = \mathbf{L}_1(\mathbf{Y} - \mathbf{C}\hat{\mathbf{X}}) \tag{34}$$

The estimation error dynamic is expressed as:

$$\dot{\tilde{\mathbf{X}}} = \dot{\mathbf{X}} - \dot{\hat{\mathbf{X}}}$$
$$\tilde{\mathbf{p}} = \dot{\mathbf{p}} - \dot{\hat{\mathbf{p}}} \tag{35}$$

By substituting Eqs. (32) and (34) into Eq. (35) and performing the calculation, we get:

$$\dot{\tilde{\mathbf{X}}} = (\mathbf{A} - \mathbf{L}_0\mathbf{C})\tilde{\mathbf{X}} + \Delta\overline{\mathbf{A}}_0\mathbf{x}_0 + \Delta\mathbf{B}a_{ym} + \Phi\tilde{\mathbf{p}} + \mathbf{H}_X\mathbf{w},$$
$$\dot{\tilde{\mathbf{p}}} = -\mathbf{L}_1\mathbf{C}\tilde{\mathbf{X}} \tag{36}$$

where

$$\Delta\overline{\mathbf{A}}_0 = \begin{bmatrix} \Delta\mathbf{A}_0 \\ \mathbf{0}_{2x2} \end{bmatrix} \tag{37}$$

A new state vector $\xi = [\tilde{\mathbf{X}}, \tilde{\mathbf{p}}, \mathbf{x}_0]^T$ is defined as follows:

$$\dot{\xi} = \mathbf{A}_p\xi + \mathbf{B}_p a_{ym} + \mathbf{H}_p\mathbf{w}, \tag{38}$$

where

4

$$\mathbf{A_p} = \begin{bmatrix} (\mathbf{A} - \mathbf{L_0C}) & \Phi & \Delta\overline{\mathbf{A}}_0 \\ -\mathbf{L_1C} & \mathbf{0_{2x2}} & \mathbf{0_{2x2}} \\ \mathbf{0_{2x4}} & \mathbf{0_{2x2}} & \mathbf{A_0} + \Delta\mathbf{A_0} \end{bmatrix} = \begin{bmatrix} (\overline{\mathbf{A}} - \mathbf{L}\overline{\mathbf{C}}) & \Delta\overline{\mathbf{A}} \\ \mathbf{0_{2x6}} & \mathbf{A_0} + \Delta\mathbf{A_0} \end{bmatrix}$$

$$\mathbf{B_p} = \begin{bmatrix} \Delta\mathbf{B} \\ \mathbf{0_{2x1}} \\ \mathbf{B_0} + \Delta\mathbf{B_0} \end{bmatrix} = \begin{bmatrix} \Delta\overline{\mathbf{B}} \\ \mathbf{B_0} + \Delta\mathbf{B_0} \end{bmatrix},$$

$$\mathbf{H_p} = \begin{bmatrix} \mathbf{H_X} \\ \mathbf{0_{2x2}} \\ \mathbf{H} \end{bmatrix} = \begin{bmatrix} \overline{\mathbf{H}} \\ \mathbf{H} \end{bmatrix} \tag{39}$$

where

$$\overline{\mathbf{A}} = \begin{bmatrix} \mathbf{A} & \Phi \\ \mathbf{0_{2x4}} & \mathbf{0_{2x2}} \end{bmatrix}$$

$$\mathbf{L} = \begin{bmatrix} \mathbf{L_0} \\ \mathbf{L_1} \end{bmatrix}$$

$$\overline{\mathbf{C}} = [\mathbf{C} \quad \mathbf{0_{2x2}}] \tag{40}$$

Next, we substitute the uncertainty terms into the function for the time-varying matrix $\mathbf{M}$:

$$\mathbf{A_p} = \begin{bmatrix} (\overline{\mathbf{A}} - \mathbf{L}\overline{\mathbf{C}}) & \overline{\mathbf{E}}_\mathbf{A}\mathbf{M_A}\mathbf{F_A} \\ \mathbf{0_{2x6}} & \mathbf{A_0} + (\mathbf{E_A}\mathbf{M_A}\mathbf{F_A}) \end{bmatrix},$$

$$\mathbf{B_p} = \begin{bmatrix} \overline{\mathbf{E}}_\mathbf{B}\mathbf{M_B}\mathbf{F_B} \\ \mathbf{B_0} + (\mathbf{E_B}\mathbf{M_B}\mathbf{F_B}) \end{bmatrix}, \tag{41}$$

where

$$\overline{\mathbf{E}}_A = \begin{bmatrix} \mathbf{E}_A \\ \mathbf{0_{4x2}} \end{bmatrix} \tag{42}$$

$$\overline{\mathbf{E}}_B = \begin{bmatrix} \mathbf{E}_B \\ \mathbf{0_{4x1}} \end{bmatrix} \tag{43}$$

Because the vehicle roll angle is the signal to be estimated, the performance of the proposed observer is evaluated based on its estimation error:

$$\tau = \mathbf{G}\xi, \tag{44}$$

where

$$\mathbf{G} = [1 \quad 0 \quad 1 \quad 0 \quad 0 \quad 0 \quad 0 \quad 0] \tag{45}$$

3.2.3. Energy-to-peak performance and stability

The systems defined in (19) and (34) are asymptotically stable and the output τ satisfies the predefined energy-to-peak performance level defined by Eq. (18). For a given γ_1 and γ_2, if there exist two matrices $\mathbf{P}$ and $\mathbf{Q}$ such that $\mathbf{P} = \mathbf{P}^T$, $\mathbf{P} > 0$, $\mathbf{Q} = \mathbf{Q}^T$, and $\mathbf{Q} > 0$, then the following inequalities are satisfied [16]:

$$\begin{bmatrix} \mathbf{PA}_p + \mathbf{A}_p^T\mathbf{P} & \mathbf{B}_p \\ * & -\mathbf{I} \end{bmatrix} < 0 \tag{46}$$

$$\begin{bmatrix} -\gamma_1^2\mathbf{I} & \mathbf{GP} \\ * & -\mathbf{P} \end{bmatrix} < 0 \tag{47}$$

$$\begin{bmatrix} \mathbf{QA}_p + \mathbf{A}_p^T\mathbf{Q} & \mathbf{I} \\ * & -\mathbf{I} \end{bmatrix} < 0 \tag{48}$$

$$\begin{bmatrix} -\gamma_2^2\mathbf{I} & \mathbf{GQ} \\ * & -\mathbf{Q} \end{bmatrix} < 0 \tag{49}$$

The difficulty in solving the above inequalities is that the matrices $\mathbf{A_p}$ and $\mathbf{B_p}$ depend on the time-varying variable $N(t)$. If we consider that the matrix $\mathbf{P}$ is defined as:

$$\mathbf{P} = \begin{bmatrix} \mathbf{P_1} & \mathbf{0} \\ * & \mathbf{P_2} \end{bmatrix} > 0, \tag{50}$$

then the inequality (46) becomes:

$$\begin{bmatrix} \mathbf{P_1}(\overline{\mathbf{A}} - \mathbf{L}\overline{\mathbf{C}}) + (\overline{\mathbf{A}} - \mathbf{L}\overline{\mathbf{C}})^T\mathbf{P_1} & \mathbf{P_1}\overline{\mathbf{E}}_A\mathbf{M}\mathbf{F}_A + (\mathbf{P_1}\overline{\mathbf{E}}_A\mathbf{M}\mathbf{F}_A)^T & \Delta\overline{\mathbf{B}} \\ * & \mathbf{P_2}(\mathbf{A_0} + \mathbf{E}_A\mathbf{M}\mathbf{F}_A) + (\mathbf{A_0} + \mathbf{E}_A\mathbf{M}\mathbf{F}_A)^T\mathbf{P_2} & (\mathbf{B_0} + \Delta\mathbf{B}) \\ * & * & -\mathbf{I} \end{bmatrix} < 0 \tag{51}$$

By continuing calculation, we get:

$$\begin{bmatrix} \mathbf{P_1}(\overline{\mathbf{A}} - \mathbf{L}\overline{\mathbf{C}}) + (\overline{\mathbf{A}} - \mathbf{L}\overline{\mathbf{C}})^T\mathbf{P_1} & \mathbf{0} & \Delta\overline{\mathbf{B}} \\ * & \mathbf{P_2}\mathbf{A_0} + \mathbf{A_0}^T\mathbf{P_2} & (\mathbf{B_0} + \Delta\mathbf{B_0}) \\ * & * & -\mathbf{I}_{1x1} \end{bmatrix}$$
$$+ \begin{bmatrix} \mathbf{P_1}\overline{\mathbf{E}}_A \\ \mathbf{P_2}\mathbf{E}_A \\ \mathbf{0} \end{bmatrix}\mathbf{M_A}[\mathbf{0} \quad \mathbf{F}_A \quad \mathbf{0}] + \begin{bmatrix} \mathbf{0} \\ (\mathbf{F}_A)^T \\ \mathbf{0} \end{bmatrix}\mathbf{M_A}[(\mathbf{P_1}\overline{\mathbf{E}}_A)^T \quad (\mathbf{P_2}\mathbf{E}_A)^T \quad \mathbf{0}] < 0 \tag{52}$$

If there are real matrices $\Omega = \Omega^T$, $\mathbf{L}$ and $\mathbf{H}$ with compatible dimensions and $N(t)$ satisfies $|N(t)| \leq 1$, then [27,28]:

$$\Omega + \mathbf{L}N(t)\mathbf{H} + \mathbf{H^T}N(t)\mathbf{L^T} < 0 \tag{53}$$

holds if and only if there exists a positive scalar ε such that:

$$\begin{bmatrix} \Omega & \mathbf{L} & \varepsilon\mathbf{H^T} \\ * & -\varepsilon\mathbf{I} & 0 \\ * & * & -\varepsilon\mathbf{I} \end{bmatrix} < 0 \tag{54}$$

For inequality (52), we consider that:

$$\Omega_A = \begin{bmatrix} \mathbf{P_1}(\overline{\mathbf{A}} - \mathbf{L}\overline{\mathbf{C}}) + (\overline{\mathbf{A}} - \mathbf{L}\overline{\mathbf{C}})^T\mathbf{P_1} & \mathbf{0} & \Delta\overline{\mathbf{B}} \\ * & \mathbf{P_2}\mathbf{A_0} + \mathbf{A_0}^T\mathbf{P_2} & (\mathbf{B_0} + \Delta\mathbf{B_0}) \\ * & * & -\mathbf{I} \end{bmatrix}$$
$$\mathbf{L}_A = \begin{bmatrix} \mathbf{P_1}\overline{\mathbf{E}}_A \\ \mathbf{P_2}\mathbf{E}_A \\ \mathbf{0} \end{bmatrix}$$
$$\mathbf{H}_A = [\mathbf{0} \quad \mathbf{F}_A \quad \mathbf{0}] \tag{55}$$

Then, inequality (52) is transformed into:

$$\begin{bmatrix} \mathbf{P_1}(\overline{\mathbf{A}} - \mathbf{L}\overline{\mathbf{C}}) \\ + (\overline{\mathbf{A}} - \mathbf{L}\overline{\mathbf{C}})^T\mathbf{P_1} & \mathbf{0}_{6x2} & \Delta\overline{\mathbf{B}} & \mathbf{P_1}\overline{\mathbf{E}}_A & \mathbf{0} \\ * & \mathbf{P_2}\mathbf{A_0} + \mathbf{A_0}^T\mathbf{P_2} & (\mathbf{B_0} + \Delta\mathbf{B_0}) & \mathbf{P_2}\mathbf{E}_A & (\varepsilon_A\mathbf{F}_A)^T \\ * & * & -\mathbf{I} & \mathbf{0} & \mathbf{0} \\ * & * & * & -\varepsilon_A\mathbf{I} & \mathbf{0} \\ * & * & * & * & -\varepsilon_A\mathbf{I} \end{bmatrix} < 0 \tag{56}$$

Eq. (56) can be rewritten as:

$$\begin{bmatrix} \mathbf{P_1}(\overline{\mathbf{A}} - \mathbf{L}\overline{\mathbf{C}}) \\ + (\overline{\mathbf{A}} - \mathbf{L}\overline{\mathbf{C}})^T\mathbf{P_1} & \mathbf{0} & \mathbf{0} & \mathbf{P_1}\overline{\mathbf{E}}_A & \mathbf{0} \\ * & \mathbf{P_2}\mathbf{A_0} + \mathbf{A_0}^T\mathbf{P_2} & \mathbf{B_0} & \mathbf{P_2}\mathbf{E}_A & (\varepsilon_A\mathbf{F}_A)^T \\ * & * & -\mathbf{I} & \mathbf{0} & \mathbf{0} \\ * & * & * & -\varepsilon_A\mathbf{I} & \mathbf{0} \\ * & * & * & * & -\varepsilon_A\mathbf{I} \end{bmatrix}$$
$$+ \begin{bmatrix} \overline{\mathbf{E}}_B \\ \mathbf{E}_B \\ \mathbf{0} \\ \mathbf{0} \\ \mathbf{0} \end{bmatrix}\mathbf{M_B}[\mathbf{0} \quad \mathbf{0} \quad \mathbf{F}_B \quad \mathbf{0} \quad \mathbf{0}] + \begin{bmatrix} \mathbf{0} \\ \mathbf{0} \\ (\mathbf{F}_B)^T \\ \mathbf{0} \\ \mathbf{0} \end{bmatrix}\mathbf{M_B}[(\overline{\mathbf{E}}_B)^T \quad (\mathbf{E}_B)^T \quad \mathbf{0} \quad \mathbf{0} \quad \mathbf{0}] < 0 \tag{57}$$

Applying inequality (54) to eliminate the time-varying matrix M_B, we get:

Table 1
Vehicle parameters and their uncertainties.

Symbol	Value	Unit
C_R	53,071	Nms/rad
m_s	1700	kg
h_{cr}	0.25	m
I_{xx}	1700	kgm^2
K_R	55,314	Nms/rad
ΔC_R	20,000	Nms/rad
Δm_s	800	kg
Δh_{cr}	0.1	m
ΔK_R	20,000	Nm/rad

$$
\begin{bmatrix}
\mathbf{P_1}(\overline{\mathbf{A}} - \mathbf{L}\overline{\mathbf{C}}) & \mathbf{0} & \mathbf{0} & \mathbf{P_1}\overline{\mathbf{E}}_A & \mathbf{0} & \overline{\mathbf{E}}_B & \mathbf{0} \\
+ (\overline{\mathbf{A}} - \mathbf{L}\overline{\mathbf{C}})^T\mathbf{P_1} & & & & & & \\
* & \mathbf{P_2}\mathbf{A}_0 + \mathbf{A}_0^T\mathbf{P_2} & \mathbf{B}_0 & \mathbf{P_2}\mathbf{E}_A & (\varepsilon_A\mathbf{F}_A)^T & \mathbf{E}_B & \mathbf{0} \\
* & * & -\mathbf{I} & \mathbf{0} & \mathbf{0} & \mathbf{0} & (\varepsilon_B\mathbf{F}_B)^T \\
* & * & * & -\varepsilon_A\mathbf{I} & \mathbf{0} & \mathbf{0} & \mathbf{0} \\
* & * & * & * & -\varepsilon_A\mathbf{I}_{2x2} & \mathbf{0} & \mathbf{0} \\
* & * & * & * & * & -\varepsilon_B\mathbf{I} & \mathbf{0} \\
* & * & * & * & * & * & -\varepsilon_B\mathbf{I}
\end{bmatrix}
$$
$$< 0 \tag{58}$$

To solve inequality (48), the matrix **Q** is defined as:

$$
\mathbf{Q} = \begin{bmatrix} \mathbf{P_1} & \mathbf{0} \\ * & \mathbf{Q_2} \end{bmatrix} > 0 \tag{59}
$$

Therefore, inequality (48) becomes:

$$
\begin{bmatrix}
\mathbf{P_1}(\overline{\mathbf{A}} - \mathbf{L}\overline{\mathbf{C}}) + (\overline{\mathbf{A}} - \mathbf{L}\overline{\mathbf{C}})^T\mathbf{P_1} & \mathbf{P_1}\overline{\mathbf{E}}_A\mathbf{M}_A\mathbf{F}_A + (\mathbf{P_1}\overline{\mathbf{E}}_A\mathbf{M}_A\mathbf{F}_A)^T & \overline{\mathbf{H}} \\
* & \mathbf{Q_2}(\mathbf{A}_0 + \mathbf{E}_A\mathbf{M}_A\mathbf{F}_A) & \mathbf{I} \\
 & + (\mathbf{A}_0 + \mathbf{E}_A\mathbf{M}_A\mathbf{F}_A)^T\mathbf{Q_2} & \\
* & * & -\mathbf{I}
\end{bmatrix} < 0 \tag{60}
$$

Following the same steps as those for inequality (51), inequality (60) becomes:

$$
\begin{bmatrix}
\mathbf{P_1}(\overline{\mathbf{A}} - \mathbf{L}\overline{\mathbf{C}}) + (\overline{\mathbf{A}} - \mathbf{L}\overline{\mathbf{C}})^T\mathbf{P_1} & \mathbf{0} & \overline{\mathbf{H}} & \mathbf{P_1}\overline{\mathbf{E}}_A & \mathbf{0} \\
* & \mathbf{Q_2}\mathbf{A}_0 + \mathbf{A}_0^T\mathbf{Q_2} & \mathbf{I} & \mathbf{Q_2}\mathbf{E}_A & (\varepsilon_C\mathbf{F}_A)^T \\
* & * & -\mathbf{I} & \mathbf{0} & \mathbf{0} \\
* & * & * & -\varepsilon_C\mathbf{I} & \mathbf{0} \\
* & * & * & * & -\varepsilon_C\mathbf{I}
\end{bmatrix} < 0 \tag{61}
$$

Furthermore, by applying:

$$
\mathbf{K} = \mathbf{P_1}\mathbf{L}, \tag{62}
$$

the inequalities (58) and (61) can be rewritten as:

$$
\begin{bmatrix}
(\mathbf{P_1}\overline{\mathbf{A}} - \mathbf{K}\overline{\mathbf{C}}) & \mathbf{0} & \mathbf{0} & \mathbf{P_1}\overline{\mathbf{E}}_A & \mathbf{0} & \overline{\mathbf{E}}_B & \mathbf{0} \\
+ (\mathbf{P_1}\overline{\mathbf{A}} - \mathbf{K}\overline{\mathbf{C}})^T & & & & & & \\
* & \mathbf{P_2}\mathbf{A}_0 + \mathbf{A}_0^T\mathbf{P_2} & \mathbf{B}_0 & \mathbf{P_2}\mathbf{E}_A & (\varepsilon_A\mathbf{F}_A)^T & \mathbf{E}_B & \mathbf{0} \\
* & * & -\mathbf{I} & \mathbf{0} & \mathbf{0} & \mathbf{0} & (\varepsilon_B\mathbf{F}_B)^T \\
* & * & * & -\varepsilon_A\mathbf{I} & \mathbf{0} & \mathbf{0} & \mathbf{0} \\
* & * & * & * & -\varepsilon_A\mathbf{I} & \mathbf{0} & \mathbf{0} \\
* & * & * & * & * & -\varepsilon_B\mathbf{I} & \mathbf{0} \\
* & * & * & * & * & * & -\varepsilon_B\mathbf{I}
\end{bmatrix}
$$
$$< 0 \tag{63}$$

$$
\begin{bmatrix}
(\mathbf{P_1}\overline{\mathbf{A}} - \mathbf{K}\overline{\mathbf{C}}) + (\mathbf{P_1}\overline{\mathbf{A}} - \mathbf{K}\overline{\mathbf{C}})^T & \mathbf{0} & \overline{\mathbf{H}} & \mathbf{P_1}\overline{\mathbf{E}}_A & \mathbf{0} \\
* & \mathbf{Q_2}\mathbf{A}_0 + \mathbf{A}_0^T\mathbf{Q_2} & \mathbf{I} & \mathbf{Q_2}\mathbf{E}_A & (\varepsilon_C\mathbf{F}_A)^T \\
* & * & -\mathbf{I} & \mathbf{0} & \mathbf{0} \\
* & * & * & -\varepsilon_C\mathbf{I} & \mathbf{0} \\
* & * & * & * & -\varepsilon_C\mathbf{I}
\end{bmatrix} < 0
$$
$$\tag{64}$$

Additionally, all the eigenvalues of the closed-loop systems defined in (19) and (34) should be constrained to a disk (k, c) with radius k and centre location ($-c$, 0) on the complex plane in order to achieve an acceptable transient response with relatively less control energy [17,29]. This condition is satisfied if there exists a positive-definite and symmetric matrix $\mathbf{P_1}$ such that the following inequality holds true:

$$
\begin{bmatrix}
-c\mathbf{P_1} & (\mathbf{P_1}\overline{\mathbf{A}} - \mathbf{K}\overline{\mathbf{C}}) + k\mathbf{P_1} \\
* & -c\mathbf{P_1}
\end{bmatrix} < 0 \tag{65}
$$

To simplify the problem, the energy-to-peak performance index γ_2 is given and the minimum energy-to-peak performance index γ_1 is obtained by solving the following minimisation problem:

$$
min\gamma_1^2, \tag{66}
$$

Which is subject to Eqs. (47), (49), (50), (59), (63), (64), and (65).

$\mathbf{P_1}$, $\mathbf{P_2}$, $\mathbf{Q_2}$, $\mathbf{K}$, ϵ_A, ϵ_B, ϵ_C, and γ_1 can be obtained by solving the above linear matrix inequality problem. Then, the observer gain $\mathbf{L}$ can be calculated by applying Eq. (62).

4. Results and discussion

To prove the effectiveness of the proposed vehicle roll angle observer, both simulations and experimental tests are performed. Table 1 lists the nominal parameters for the vehicle model described in Section 2 with their maximum uncertainties taken into account.

By solving the minimisation problem in (66) for the observers defined by Eqs. (19) and (34) for a value of the energy-to-peak performance index γ_2 equal to 1 and a constrained disk (100,100), the obtained observer gains are listed in Table 2. For observer 2, two filter gains are taken into account: $\mathbf{F} = 5$ and $\mathbf{F} = 10$. We observed that the values of the energy-to-peak performance index obtained for both observers were very similar.

In the following sections, the simulation and experimental results obtained for both observers are described for different manoeuvres.

4.1. Simulation results

The simulation tests were conducted using a vehicle simulation model from TruckSim, which has been validated using real test data

Table 2
Energy-to-peak performance indexes and observer gains for observer 1 and observer 2.

	Contraint disk (k,c)	Filter gain F	Observer gain γ_1	L
Observer 1	(100,100)	–	0.05	[199.9971 1.1834 −73.6383 37.4894]
Observer 2	(100,100)	10	0.0501	[199.7189 24.0120 −73.6383 18.7519 210.7189 37.5028 0.0000 18.5493 0.0000 0.4928 0.0000 0.8994]
	(100,100)	5	0.0504	[199.0945 −3721.3 −73.6381 3687.4 205.0946 −112.4065 0.0000 92.8065 0.0000 4.2153 0.0000 12.2064]

obtained from a real vehicle [7]. The use of a vehicle model allowed us to perform different vehicle manoeuvres under different road conditions without putting human lives at stake. Additionally, simulation models guarantee test reproducibility. In order to simulate the information provided by an IMU sensor, a sensor was defined at the COG of the vehicle simulation model.

To analyse the effect that sensor measurement noises have on the estimation of vehicle roll angle, Gaussian noises with zero mean and variances of 0.01 g's, 0.01 g's, 0.01 deg/s, and 0.01 0.01 deg/s were added to the values of a_x (longitudinal acceleration), a_y (lateral acceleration), r (yaw rate), and $\dot{\phi}$ (roll rate), respectively, obtained from TruckSim.

The proposed vehicle roll angle observers were evaluated using a slalom manoeuvre with a vehicle speed defined by a ramp function profile (from 10 km/h to 120 km/h in 120 s) and sine sweep manoeuvre at 40 km/h. Both tests were performed on road surfaces with friction coefficients of 0.5 (wet) and 0.85 (dry).

To demonstrate the necessity of the integration of an NN with energy-to-peak filtering for vehicle roll angle estimation, different cases are analysed:

- Vehicle roll angle estimation obtained directly from the NN ϕ_{NN} without filtering.
- Vehicle roll angle estimation considering a 'pseudo-roll angle' obtained from the NN module ϕ_{NN}, where the roll rate signal $\dot{\phi}$ is provided by the IMU, in combination with energy-to-peak filtering. In this case:

$$\mathbf{y_{meas}} = [\phi_{NN} \quad \dot{\phi}]^{\mathbf{T}} \tag{67}$$

$$\mathbf{C_0} = \begin{bmatrix} 1 & 0 \\ 0 & 1 \end{bmatrix} \tag{68}$$

- Vehicle roll angle estimation using energy-to-peak filtering and considering that only the roll rate signal $\dot{\phi}$ is available. In this case:

$$\mathbf{y}_{meas} = [\dot{\phi}]^T \tag{69}$$

$$\mathbf{C_0} = [0 \quad 1] \tag{70}$$

In Figs. 4 and 5, the results for a slalom manoeuvre with a vehicle speed defined by a ramp function profile on pavement with a friction coefficient of 0.85 and sine sweep manoeuvre at 40 km/h on pavement with a friction coefficient of 0.5 are presented, respectively. In both figures, one can see that the roll angle obtained directly from the NN module is strongly affected by signal noise (red colour). The use of energy-to-peak observers in combination with the NN module reduces this effect. Additionally, the estimation of vehicle roll angle is not accurate if it only considers the measurement from the yaw rate sensor (light blue colour). In order to quantify the accuracy of the proposed algorithms, norm and maximum errors were calculated. The equation used to calculate the norm error as a function of time is [30]:

$$E_t = \frac{\varepsilon_t}{\sigma_t}, \tag{71}$$

where

$$\varepsilon_t^2 = \int_0^T (\phi_{exp} - \phi_{est})^2 \, dt$$

$$\sigma_t^2 = \int_0^T (\phi_{exp} - \mu_{exp})^2 \, dt \tag{72}$$

ϕ_{exp} represents the real vehicle roll angle, ϕ_{est} represents the vehicle roll angle obtained from the observer, and μ_{exp} is the mean value of the real vehicle roll angle obtained during the period T.

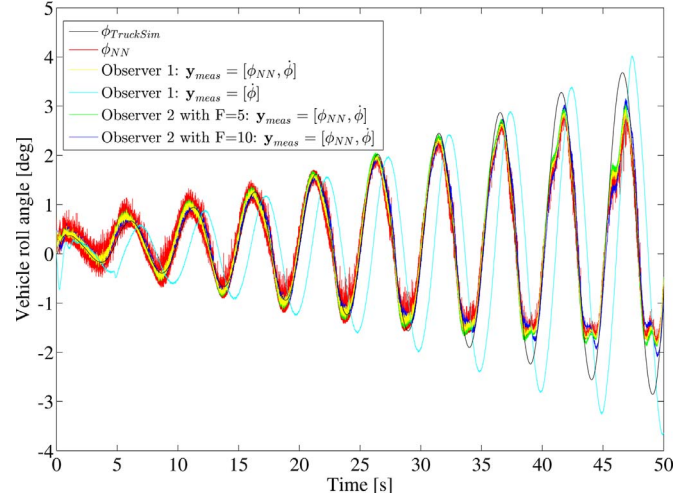Tables 3 and 4 list the norm and maximum errors values for a slalom

Fig. 4. Simulation results for a slalom manoeuvre with a vehicle speed defined by a ramp function profile on pavement with a friction coefficient of 0.85. (For interpretation of the references to colour in this figure legend, the reader is referred to the web version of this article.)

Fig. 5. Simulation results for a sine sweep manoeuvre at 40 km/h on pavement with a friction coefficient of 0.5. (For interpretation of the references to colour in this figure legend, the reader is referred to the web version of this article.)
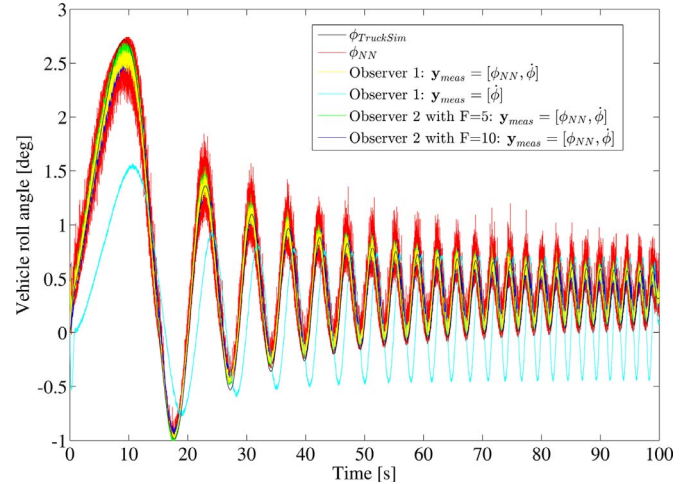
Table 3
Norm and maximum errors for slalom manoeuvre with a vehicle speed defined by a ramp function profile.

CASE	Friction coefficient			
	0.5		0.85	
	Norm error E_t	Max. error E_{max} (deg)	Norm error E_t	Max. error E_{max} (deg)
1: NN	0.305	2.868°	0.254	2.372°
2: NN + observer 1	0.294	2.547°	0.241	1.727°
3: observer 1	1.048	5.609°	1.064	3.583°
4: NN + observer 2 with F = 5	**0.283**	2.511°	**0.228**	**1.636°**
5: NN + observer 2 with F = 10	0.306	**2.456°**	0.256	1.856°

manoeuvre with vehicle speed defined by a ramp function profile and sine sweep manoeuvre at 40 km/h, respectively, on road surfaces with friction coefficients of 0.5 (wet) and 0.85 (dry). It should be noted that if only the signal of the yaw rate sensor is considered (case 3), the estimation of vehicle roll angle is not very accurate. The use of the NN

Table 4
Norm and maximum errors for a sine sweep manoeuvre at 40 km/h.

CASE	Friction coefficient			
	0.5		0.85	
	Norm error E_t	Max. error E_{max} (deg)	Norm error E_t	Max. error E_{max} (deg)
1: NN	0.179	0.728°	0.188	0.728°
2: NN + observer 1	**0.109**	**0.563°**	0.119	**0.563°**
3: observer 1	0.796	1.362°	0.812	1.370°
4: NN + observer 2 with F = 5	**0.109**	0.580°	**0.113**	0.580°
5: NN + observer 2 with F = 10	0.115	0.601°	0.125	0.601°

module to estimate vehicle roll angle is a better solution. However, as indicated previously, the NN module is strongly affected by sensor noise. The use of an energy-to-peak-based observer reduces the effect of noise (cases 2, 4, and 5). The observers with the best performance are those that combine the NN with observers 1 and 2, with a gain filter of 5.

4.2. Experimental results

Experimental tests were performed using a Mercedes Benz Sprinter van. This real van was equipped with a VBOX 3i dual-antenna data logger, two GPS dual-antennas and an IMU sensor (Fig. 6). The two GPS antennas were mounted on vehicle to measure the real vehicle roll angle. Therefore, this value is used as the ground truth. The ground truth is used to prove the effectiveness of the proposed algorithm.

The real test was performed on dry pavement at a speed of 40 km/h for a combination of severe J-turn and slalom manoeuvres. Fig. 7 presents a comparison of the values of vehicle roll angle obtained directly from the GPS dual-antenna (black color), NN module (green color), combination of NN + observer 1 (red color), and observer 1 considering only the yaw rate signal (purple color). Fig. 8 presents a comparison of the results obtained directly from the GPS dual-antenna (black color), NN module (green color), combination of NN + observer 2 with a filter gain value of 5 (red color), and combination of NN + observer 2 with a filter gain value of 10 (blue color). In Table 5, the norm and maximum errors are listed for the different proposed observers. The results indicate that it is necessary to estimate the 'pseudo-roll angle' from the NN module in order to improve vehicle roll angle estimation. From experimental results, the observer system achieves the best performance when combining the NN with observer 1. However, the reduction in measurement noise is less significant in observer 1 because various disturbances, such as road irregularities, can strongly affect sensor signals.
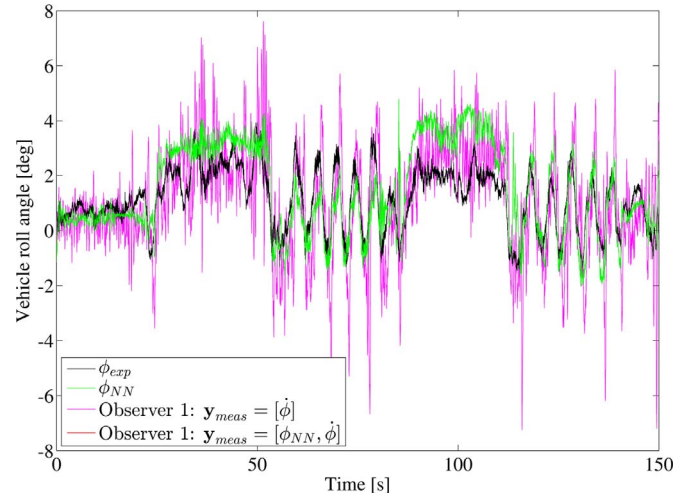

Fig. 6. Real vehicle used for experiments.

Fig. 7. Comparison of experimental results for NN + observer 1: results from GPS dual-antenna (black color), results from NN module (green color), results from the combination of NN + observer 1 (red color), and results from observer 1 considering only the yaw rate signal (purple color). (For interpretation of the references to colour in this figure legend, the reader is referred to the web version of this article.)
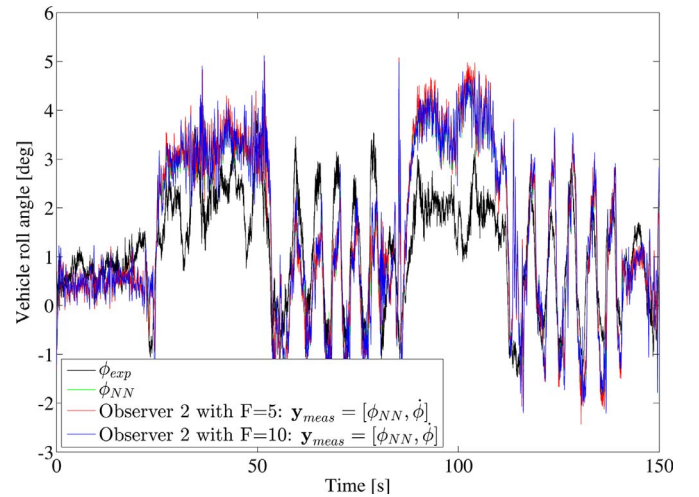

Fig. 8. Comparison of experimental results for NN + observer 2: results from GPS dual-antenna (black color), results from NN module (green color), results from the combination of NN + observer 2 with a filter gain value of 5 (red color), and results from the combination of NN + observer 2 with a filter gain value of 10 (blue color). (For interpretation of the references to colour in this figure legend, the reader is referred to the web version of this article.)

Table 5
Norm and maximum errors for the real test.

CASE	Norm error	Maximum error
	E_t	E_{max} (rad, deg)
1: NN	1.052	0.096°
2: NN + observer 1	**1.051**	**0.095°**
3: observer 1	1.531	0.149°
4: NN + observer 2 with F = 5	1.102	0.101°
5: NN + observer 2 with F = 10	1.128	0.099°

5. Conclusion

In this paper, we present a novel observer system based on a combination of an NN and energy-to-peak-based observer. The NN estimates a 'pseudo-roll angle' from sensor signals that can be obtained in current vehicles. The NN acts a 'pseudo-sensor' whose estimates are

introduced as measurements in the energy-to-peak-based observer.

Both simulation and experimental results demonstrate that it is necessary to utilise the 'pseudo-roll angle' estimated by the NN module in order to obtain good performance at estimating vehicle roll angle.

The results prove that it is possible to design an observer that guarantees convergence and system stability using only measurements provided by the sensors installed in current vehicles, without requiring GPS information or any knowledge of system or sensor noise.

Acknowledgement

References

[1] Rajamani R, Piyabongkarn DN. New paradigms for the integration of yaw stability and rollover prevention functions in vehicle stability control. IEEE Trans Intell Transp Syst 2013;14(1):249–61. http://dx.doi.org/10.1109/TITS.2012.2215856.

[2] Boada MJL, Boada BL, Gauchia A, Calvo JA, Diaz V. Active roll control using reinforcement learning for a single unit heavy vehicle. Int J Heavy Veh Syst 2009;16(4):412–30.

[3] Li B, Du H, Li W, Zhang Y. Side-slip angle estimation based lateral dynamics control for omni-directional vehicles with optimal steering angle and traction/brake torque distribution. Mechatronics 2015;30:348–62. http://dx.doi.org/10.1016/j.mechatronics.2014.12.001.

[4] Jo K, Chu K, Sunwoo M. Interacting multiple model filter-based sensor fusion of gps with in-vehicle sensors for real-time vehicle positioning. IEEE Trans Intell Transp Syst 2012;13(1):329–43. http://dx.doi.org/10.1109/TITS.2011.2171033.

[5] Bevly DM, Ryu J, Gerdes JC. Integrating ins sensors with gps measurements for continuous estimation of vehicle sideslip, roll, and tire cornering stiffness. IEEE Trans Intell Transp Syst 2006;7(4):483–93. http://dx.doi.org/10.1109/TITS.2006.883110.

[6] Doumiati M, Baffet G, Lechner D, Victorino A, Charara A. Embedded estimation of the tire/road forces and validation in a laboratory vehicle. In Proceedings of 9th International Symposium on Advanced Vehicle Control. 2008. p. 533–8.

[7] Vargas-Melendez L, Boada B, Boada M, Gauchia A, Diaz V. A sensor fusion method based on an integrated neural network and Kalman filter for vehicle roll angle estimation. Sensors 2016;16(9). http://dx.doi.org/10.3390/s16091400.

[8] Rajamani R, Piyabongkarn D, Tsourapas V, Lew JY. Parameter and state estimation in vehicle roll dynamics. IEEE Trans Intell Transp Syst 2011;12(4):1558–67. http://dx.doi.org/10.1109/TITS.2011.2164246.

[9] Nam K, Oh S, Fujimoto H, Hori Y. Estimation of sideslip and roll angles of electric vehicles using lateral tire force sensors through rls and Kalman filter approaches. IEEE Trans Ind Electron 2013;60(3):988–1000. http://dx.doi.org/10.1109/TIE.2012.2188874.

[10] Zhang S, Yu S, Liu C, Yuan X, Liu S. A dual-linear Kalman filter for real-time orientation determination system using low-cost mems sensors. Sensors 2016;16:264.

[11] Boada B, Garcia-Pozuelo D, Boada MJL, Diaz V. A constrained dual Kalman filter based on pdf truncation for estimation of vehicle parameters and road bank angle: analysis and experimental validation. IEEE Trans Intell Transp Syst 2016;PP (99):1–11. http://dx.doi.org/10.1109/TITS.2016.2594217.

[12] Yu B, Shi Y, Huang H. $l_2 - l_\infty$ filtering for multirate systems based on lifted models. Circuits Syst Signal Process 2008;27(5):699–711. http://dx.doi.org/10.1007/s00034-008-9058-3.

[13] Zhang H, Wang J. Vehicle lateral dynamics control through afs/dyc and robust gain-scheduling approach. IEEE Trans Veh Technol 2016;65(1):489–94. http://dx.doi.org/10.1109/TVT.2015.2391184.

[14] Zhang G, Zhang H, Huang X, Wang J, Yu H, Graaf R. Active fault-tolerant control for electric vehicles with independently driven rear in-wheel motors against certain actuator faults. IEEE Trans Control Syst Technol 2016;24(5):1557–72. http://dx.doi.org/10.1109/TCST.2015.2501354.

[15] Ferjani A, Ghorbel H, Chaabane M, Rabhi A, Elhajjaji A. Energy-to-peak performance of motorcycle lateral dynamic study. 2016 5th International Conference on Systems and Control (ICSC). 2016. p. 49–54. http://dx.doi.org/10.1109/ICoSC.2016.7507048.

[16] Zhang H, Huang X, Wang J, Karimi HR. Robust energy-to-peak sideslip angle estimation with applications to ground vehicles. Mechatronics 2015;30:338–47. http://dx.doi.org/10.1016/j.mechatronics.2014.08.003.

[17] Zhang G, Yu Z, Wang J. Correction of contaminated yaw rate signal and estimation of sensor bias for an electric vehicle under normal driving conditions. Mech Syst Signal Process 2017;87, Part B:64–80. http://dx.doi.org/10.1016/j.ymssp.2016.05.034.

[18] Hashemi E, Khosravani S, Khajepour A, Kasaiezadeh A, Chen S-K, Litkouhi B. Longitudinal vehicle state estimation using nonlinear and parameter-varying observers. Mechatronics 2017;43:28–39. http://dx.doi.org/10.1016/j.mechatronics.2017.02.004.

[19] Melzi S, Sabbioni E. On the vehicle sideslip angle estimation through neural networks: numerical and experimental results. Mech Syst Signal Process 2011;25(6):2005–19. http://dx.doi.org/10.1016/j.ymssp.2010.10.015.

[20] Boada B, Boada M, Gauchia A, Olmeda E, Diaz V. Sideslip angle estimator based on anfis for vehicle handling and stability. J Mech Sci Technol 2015;29(4):1473–81. http://dx.doi.org/10.1007/s12206-015-0320-x.

[21] Boada B, Boada M, Diaz V. Vehicle sideslip angle measurement based on sensor data fusion using an integrated anfis and an unscented Kalman filter algorithm. Mech Syst Signal Process 2016;7273:832–45. http://dx.doi.org/10.1016/j.ymssp.2015.11.003.

[22] Xu Y, Lu R, Shi P, Tao J, Xie S. Robust estimation for neural networks with randomly occurring distributed delays and Markovian jump coupling. IEEE Trans Neural Netw Learn Syst 2017;PP(99):1–11. http://dx.doi.org/10.1109/TNNLS.2016.2636325.

[23] Xu Y, Wang Z, Yao D, Lu R, Su CY. State estimation for periodic neural networks with uncertain weight matrices and Markovian jump channel states. IEEE Trans Syst Man Cybern 2017;PP(99):1–10. http://dx.doi.org/10.1109/TSMC.2017.2708700.

[24] TruckSim. http://carsim.com/products/trucksim/; 2017.

[25] Zhu X, Zhang H, Cao D, Fang Z. Robust control of integrated motor-transmission powertrain system over controller area network for automotive applications. Mech Syst Signal Process 2015;5859:15–28. http://dx.doi.org/10.1016/j.ymssp.2014.11.011.

[26] Zhang G, Yu Z, Wang J. Linear parameter-varying observer design for vehicle yaw rate sensor bias estimation and signal reconstruction. 2016 American Control Conference (ACC). 2016. p. 2391–6.

[27] Xie L, Soh YC. Robust control of linear systems with generalized positive real uncertainty. Automatica 1997;33(5):963–7. http://dx.doi.org/10.1016/S0005-1098(96)00247-6.

[28] Jiang X, Han Q-L. Delay-dependent robust stability for uncertain linear systems with interval time-varying delay. Automatica 2006;42(6):1059–65. http://dx.doi.org/10.1016/j.automatica.2006.02.019.

[29] Zhang H, Zhang X, Wang J. Robust gain-scheduling energy-to-peak control of vehicle lateral dynamics stabilisation. Veh Syst Dyn 2014;52(3):309–40. http://dx.doi.org/10.1080/00423114.2013.879190.

[30] Boada M, Calvo J, Boada B, Diaz V. Modeling of a magnetorheological damper by recursive lazy learning. Int J Non Linear Mech 2011;46(2):479–85. http://dx.doi.org/10.1016/j.ijnonlinmec.2008.11.019.

Beatriz L. Boada received her Industrial Engineering and doctoral degrees from Universidad Carlos III de Madrid (UC3M) in 1996 and 2002, respectively. She was a research assistant in the Department of Systems and Automation Engineering at UC3M from 1997 to 2002. She has worked in the localization and mapping problems in the field of robotic. Currently, she is a professor in the Mechanical Engineering Department at UC3M. Her research field covers intelligent vehicles, both autonomous and motorized, and control of vehicle in vertical and lateral dynamics. She also researches in magnetorheological damper, modelling and estimation of mechanical systems.

Maria Jesus L. Boada received her Industrial Engineering and doctoral degrees from UC3M in 1996 and 2002, respectively. She was research assistant in the Department of Systems and Automation Engineering at UC3M between 1997 and 2002. She has worked in control architectures and development of learning skills in autonomous mobile robots. She is currently a professor in the UC3M Mechanical Engineering Department. Her research area includes intelligent vehicles, both autonomous and motorized, control of vehicle lateral dynamics and magnetorheological damper.

Vicente Diaz is full professor in the Mechanical Engineering Department of UC3M and head of the research group MECATRAN. His area of expertise at UC3M is in the field of transports, vehicle dynamics engineering, end-of-life recycling and motor vehicle inspection. He has a large number of publications and papers indexed in JCR in the areas of vehicle dynamic modelling (including heavy vehicle), vehicle lateral control and tyre modelling. He has headed of projects developed for the automobile industry as well as being a leader in tyre research competitive government projects. In addition, he has supervised several PhD theses on bus structure dynamics, tyre modelling and Electronic Stability Control for automobile vehicles.